STUDY OF THE ENERGY COMPRESSION SCHEME TO ENERGY RECOVER AN ELECTRON BEAM IN PRESENCE OF AN FEL INTERACTION*

Ph. Piot †, D.R. Douglas, G.A. Krafft
Thomas Jefferson National Accelerator Facility, Newport News, VA 23606 USA

Abstract

Energy recovering an electron beam after it has participated in a free-electron laser (FEL) interaction can be quite challenging because of the substantial FEL-induced energy spread. In the Jefferson Lab infrared FEL driver-accelerator, such an energy recovery scheme has been implemented by properly matching the longitudinal phase space throughout the recirculation transport by employing the so-called energy compression scheme [1]. In the present paper, after presenting a single-particle dynamics approach of the method used to energy-recover the electron beam, we report on experimental validation of the method obtained by measurements of the phase-phase and energy-phase lattice transfer maps at different locations along the recirculation transport line. We also compare these measurements with numerical tracking simulations.

1 BACKGROUND

In the JLab IR-demo FEL, energy recovery of an electron beam after it has participated to an FEL interaction was demonstrated using the so-called same-cell energy-recovery scheme (SCER) [2]. Such a technique presents many Beam Dynamics challenges principally related (1) to energy jitter induced-instability [3], and (2) to proper longitudinal phase space manipulation (the object of the present paper). The latter point results from the relative energy spread, δ, induced by the FEL process: typically $\langle\delta^2\rangle^{1/2} \simeq 4\%$ in the present case. This substantial energy spread may induce large beam size in the dispersive sections of the recirculator and energy-recovery dump-line which in turn may yield partial beam scraping on the beam vacuum chamber, an undesired effect especially when operating with high average current ($I \simeq 5$ mA) beam. A complete description of the driver-accelerator can be found in References [1, 2]; in terms of longitudinal dynamics, the first matching point is at the wiggler location where a waist (minimum bunch length) is required. Given the longitudinal phase space at the injector front-end, the superconducting radio-frequency (SRF) linac, which consists of eight 5-cell CEBAF-type cavities, has to be tuned in amplitude (to provide a proper energy on which the laser wavelength is highly dependent) and in phase for achieving the desired longitudinal phase space correlation, $\simeq d\delta/dz$, to match the momentum compaction R_{56}^C of the first chicane (which thereby acts as a bunch compressor) accordingly to the "maximum compression" condition: $d\delta/dz|_{z=0} = -1/R_{56}^C$. In the nominal operating conditions the aforementioned requirements results in operating the linac $-8\,\mathrm{deg}$ off crest for an accelerating voltage of approximately $37\,\mathrm{MeV}$. Downstream of the wiggler the transport consists of (1) a magnetic chicane similar to the one aforementioned, $R_{56}^C \simeq 30$cm, which acts as a bunch decompressor, and (2) two identical 180 deg arcs providing tunable path length, and linear, R_{56}^A, as well as quadratic , T_{566}^A, momentum compaction. Adjustement of the linear (resp. quadratic) momentum compaction is possible via two pairs of quadrupole (resp. sextupole) located in each arc. After the recirculation transport the beam is re-injected in the SRF linac on the deceleration phase (i.e. $-8 + 180\,\mathrm{deg}$ under nominal operation) so that when decelerated, the electromagnetic energy induced via beam loading stored in the cavities is directly used to supplement the available power for the accelerating mode. Under the single-particle-dynamics approximation, the recirculator can be modeled by the longitudinal map $\mathcal{Z}$ which maps an electron with initial coordinate (z_i, δ_i) at the undulator exit to the exit of the linac after deceleration (z_f, δ_f):

$$z_i \xrightarrow{\mathcal{Z}} z_f = (R_{55} + \sum_j T_{55j}) z_i + T_{555} z_i^2 + (R_{56} + \sum_j T_{56j})\delta_i + T_{566}\delta_i^2 + ..., \text{ and } \delta_i \xrightarrow{\mathcal{Z}} \delta_f = R_{65} z_i + R_{66}\delta_i \quad (1)$$

In Eqns.(1) the first and second order transfer matrix elements are between the wiggler and the linac exit so that $R_{66} = R_{66}^{linac} + R_{65}^{linac} R_{56}^{i\rightarrow f}$. Since R_{65}^{linac} is fixed, the only way of varying the energy spread is to act on $R_{56}^{i\rightarrow f} = R_{56}^C + 2R_{56}^A$, the same type of remark applies for $T_{566}^{i\rightarrow f}$. We illustrate the energy compression scheme in Figure 1, by tracking a PARMELA-generated longitudinal phase space using the Eqns.(1) augmented by an RF model which includes RF-curvature effects.

2 EXPERIMENT AND SIMULATION FOR THE IR-DEMO

The experiment essentially consists of characterizing the "compression" transfer map, i.e. $\partial\phi_f/\partial\phi_i$, between the photocathode (i) and a pickup cavity (f), and the "momentum compaction" transfer map, i.e. $\partial\phi_f/\partial\delta_i$, between the last cavity of the SRF linac (i) and a pickup cavity (f); with $\phi_{(i,f)} = (2\pi/\lambda) z_{(i,f)}$, λ being the RF-wavelength. In fact a transfer map measurement reduces to a time-of-flight (TOF) measurement.

* This work was performed under the auspices of the US-DOE contract #DE-AC05-84ER40150, the Office of Naval Research, the Commonwealth of Virginia, and the Laser Processing Consortium.

† Now at Deutsches Elektronen-Synchrotron DESY Hamburg, Germany

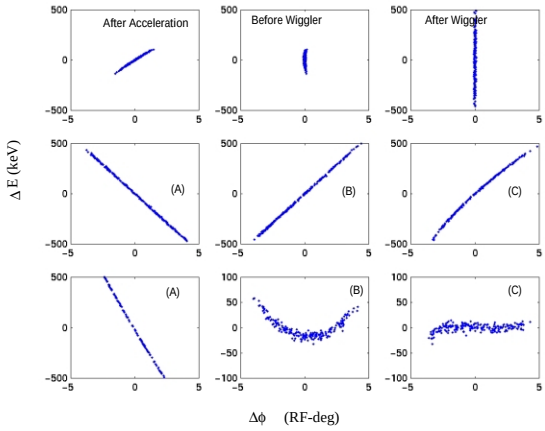

Figure 1: Energy compression scheme: The first row (from left to right) presents the longitudinal phase space at the linac exit, after the compression chicane, and just after the wiggler interaction (i) has taken place; the second row show longitudinal phase space at the entrance of the linac (f) just prior to deceleration for three different senarii of $R_{56}^{i\to f}$ and $T_{566}^{i\to f}$ (for (**A**) -0.2 and 0. m, for (**B**) 0.2 and 0 m and for (**C**) 0.2 and 3.0 m). The result for each of the three cases in the second row are shown in the third row after deceleration.

2.1 *experimental setup*

Measurement of TOF is performed by detecting the amplitude signal produced by the TM_{010} waves excited as the electron traverses a resonant stainless steal cavity [4, 5]. The cavity has a resonant frequency of 1.497 GHz. The principle of the TOF measurement is to measure the phase of beam induced voltage since it is in phase with the bunch. The phase of the RF signal coming from the cavity $V_{RF}\cos(\omega t+\phi_{RF})$ is mixed with the reference signal phase shifted by the mean of a programmable phase shifter $V_0\cos(\omega t+\phi_0)$. The signal at the mixer output, after removal of high frequency component with a low pass filter, is: $V_{out}=V_{RF}V_0/2\sin\Delta\phi$, where $\Delta\phi=\phi_{RF}-\phi_0$ is a measure of the relative TOF. The coefficient $(V_{RF}V_0)/2$ is initially determined during a calibration procedure that consists of varying the phase shifter to find the zero-crossings of the pickup cavity, i.e. the phase for which the signal V_{out} is zero. Once the measurement is calibrated, the phase shifter phase ϕ_0 is set so that for the nominal conditions of the machine the cavity is operated at zero-crossing. Hence a change in the TOF induced by varying the phase of the photo-cathode drive laser (for $\partial\phi_f/\partial\phi_i$ map measurement) or by an energy change (for $\partial\phi_f/\partial\delta_i$ map measurement) gives a change of ϕ_{RF} which in turn induce a change of V_{out}. Practically only the change in V_{out} is directly measured but because one knows the coefficient $V_{RF}V_0$ one can infers ϕ_{RF} i.e. the TOF of the bunch. In the recirculating linac, three cavities have been installed; their locations are: downstream of (1) the main SRF-linac, the (2) first and (3) second 180 deg arc. These pickup cavities will be referred as #2, #3 and #4 henceforth. To expedite the measurements, the quantity varied (i.e. laser phase for $\partial\phi_f/\partial\phi_i$ transfer map and cavity gradient for $\partial\phi_f/\partial\delta_i$ transfer map), is changed at 60 Hz.

2.2 *the numerical model*

As aforementioned the measurement of phase-phase transfer map provides important information on how the bunching process is performing and can give some insights on the bunch length. Because the map is measured between the photocathode and the pickup cavities, we cannot use standard single particle dynamics relativistic codes, but need to use particle tracking code, e.g., PARMELA [6] which include non relativistic effects such as phase slippage effects in accelerating cavities. The technique we have used to compare measurement with numerical simulation is as follows: we use PARMELA to generate uniform macroparticle distribution over a given extent in phase at the photocathode surface. The corresponding phase of emission ϕ_i^k of the k-th macroparticle at the photocathode surface is recorded and the macroparticles populating this uniform distribution are tracked along the beamlines. During the tracking the space charge subroutine is deactivated, and each macroparticle is assumed to be the bunch centroid of bunches emitted at different drive-laser phase, we then compute the phase of arrival ϕ_f^k at the desired pickup cavities. The couple $(\{\phi_i^k,\ \phi_f^k\}_{k=1,\ldots,N})$ directly gives the phase-phase transfer map which can be compared to the experimental data. In order to generate energy-phase transfer maps, we use the arbitrary high order code TLIE [7] based on a simplectic integrator: the energy offsets achieved when modulating the gradient of the last cryomodule cavity is directly used by the code to calculate the TOF up to one of the pickup cavity. The couple $(\{\delta_i^k,\ \phi_f^k\}_{k=1,\ldots,N})$ provides the energy-phase correlation and again can be compared with the data.

2.3 *comparison experiment/simulation*

Compression efficiency: In Figure 2, we present typical measurement of the $\partial\phi_f/\partial\phi_i$ maps at the three different cavities: we generally observe good agreement with the expectations from simulation; the slight disagreement observed for cavity #4, being attributed to a bad centering of the electron beam on the magnetic axis of the trim quadrupoles and sextupoles in arc #2 during our experiment. Performing a nonlinear fit of the transfer function presented in the Figure can give some insight on the linear R_{55} and nonlinear, T_{555} compression efficiency coefficients between the photocathode and the pickup cavities: the results are presented in Table 1.

Momentum compaction: From the measurement of the energy-phase transfer map, we have computed the momentum compaction values for the recirculation loop, i.e. from the wiggler up to the exit of the second arc. Figure 3 compares the results with expected values obtained with the second order optics code DIMAD [8], the agreement is

Pickup	Linear Coeff.	Quadratic Coeff.
Experiment		
# 2	0.1172	0.0008
# 3	-0.0801	0.0016
# 4	0.0911	0.0006
Simulation		
# 2	0.1070	0.0007
# 3	-0.0834	0.0003
# 4	0.0256	0.0004

Table 1: Comparison of coefficients obtained from the non-linear fit of the measured and PARMELA-simulated $\partial\phi_F/\partial\phi_i$ transfer map.

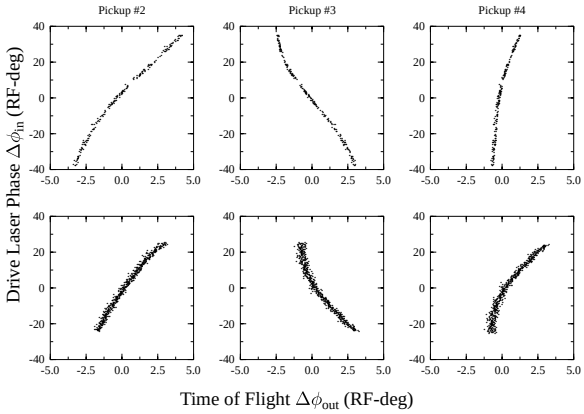

Figure 2: Comparison of the phase-phase beam transfer function between the photocathode surface and the three different pickup cavities (pickup #2, #3, and #4) **(bottom row)** with the one simulated using PARMELA **(top row)**.

very good. We have a good way of setting up the arcs to match the R_{56} of Eqns.(1) to the required value for achieving energy compression.

Other experimental evidence of energy compression: An evidence of the good performance of the energy compression scheme was our ability to recover 5 mA average current beam while lasing at high gain with an average output power of 1.7 kW without any beamlosses. Another validation of the method is to observe (see Fig.4) the beam spot on the energy recovery dump window: when the longitudinal compression is properly tuned the beam is tightly focussed whereas by slightly mis-setting the one pairs of sextupole (which does not affect – to first order – the lattice functions), the beam horizontal (dispersive) direction starts to blow-up.

3 CONCLUSION

In summary, we have successfully characterized the energy compression scheme to recover the spent electron beam after the FEL-process in the IR-demo. Such techniques are well adapted for energy-recovering an electron beam in a moderate power FEL. For the foreseen 10 kW upgrade, higher (e.g. third) order corrections must be considered, and the use of a dedicated "accelerating" section for the energy compression is envisaged. As far as operation of the IR-FEL demo, the transfer maps measurements have shown to be a very fast and valuable tool for setting up the accelerator in a reproducible way.

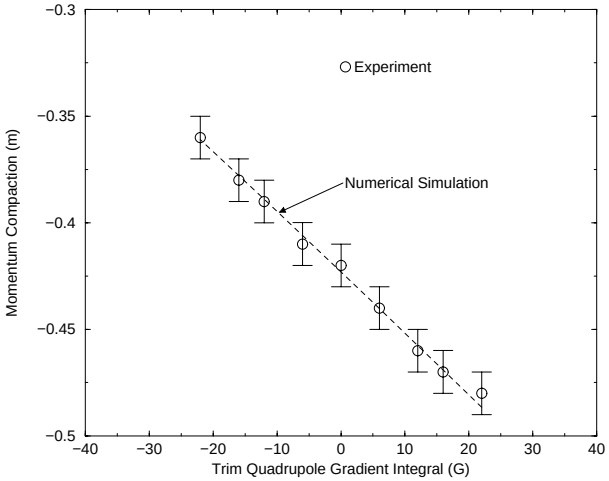

Figure 3: Comparison between the expected and measured linear momentum compaction, R_{56}, for the whole recirculation transport, versus different settings for one of the trim quadrupole pairs in one of the 180-deg arc.

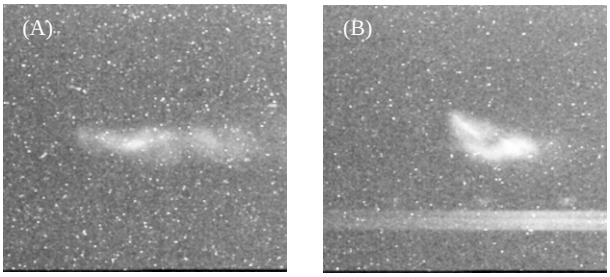

Figure 4: Beam spot changes when the sextupoles in the recirculating arcs are turned off (**left**) and excited to their nominal values (**right**) .

4 REFERENCES

[1] Douglas D.R., Proc. Part. Acc. Conf 97 IEEE cat.# 97CH36167, pp. 1351-1355 (1997)

[2] Neil G. R., et al., *Phys. Rev. Lett.*, vol. 84, num. 4, pp. 662-665 (2000)

[3] Merminga L., et al. Nucl. Instr. Meth. **A 429**, pp. 58-64 (1999)

[4] Krafft G. A., AIP conf. proc. 367, pp. 46-55 (1995)

[5] Hardy D., Ibid [1], pp. 2265-2267 (1997)

[6] H. Liu, private communication, code written by K. Crandall.

[7] van Zeijt J., TLIE code, private communication

[8] Sevranckx R.V., et al. SLAC report **285**, (1985)